**Steel and Composite Structures**, *Vol. 30, No. 2 (2019) 81-96*
DOI: https://doi.org/10.12989/scs.2019.30.2.081


# Behavior of three-tube buckling-restrained brace with circumference pre-stress in core tube

Yang Li [1], Haiyan Qu [2], Shaowen Xiao [1,3], Peijun Wang [*1], Yang You [1] and Shuqing Hu [**4]

[1] *Civil Engineering College of Shandong University, Jinan, Shandong Province, 250061, China*
[2] *Technical Center of Zhongnan Building Industry Group, Nantong, Jiangsu Province, 226100, China*
[3] *Headquarters of China Vanke Co. Ltd., Guangzhou, Guangdong Province, 510000, China*
[4] *Technical Center of Zhongtong Steel Construction Co., Ltd., Liaocheng, Shandong Province, 252000, China*

(*Received March 18, 2018, Revised November 12, 2018, Accepted January 15, 2019*)

**Abstract.** The behavior of a new Three-Tube Buckling-Restrained Brace (TTBRB) with circumference pre-stress ($\sigma_{\theta,pre}$) in core tube are investigated through a verified finite element model. The TTBRB is composed of one core tube and two restraining tubes. The core tube is in the middle to provide the axial stiffness, to carry the axial load and to dissipate the earthquake energy. The two restraining tubes are at inside and outside of the core tube, respectively, to restrain the global and local buckling of the core tube. Based on the yield criteria of fringe fiber, a design method for restraining tubes is proposed. The applicability of the proposed design equations are verified by TTBRBs with different radius-thickness ratios, with different gap widths between core tube and restraining tubs, and with different levels of $\sigma_{\theta,pre}$. The outer and inner tubes will restrain the deformation of the core tube in radius direction, which causes circumference stress ($\sigma_{\theta}$) in the core tube. Together with the $\sigma_{\theta,pre}$ in the core tube that is applied through interference fit of the three tubes, the yield strength of the core tube in the axial direction is improved from 160 MPa to 235 MPa. Effects of gap width between the core tube and restraining tubes, and $\sigma_{\theta,pre}$ on hysteretic behavior of TTBRBs are presented. Analysis results showed that the gap width and the $\sigma_{\theta,pre}$ can significantly affect the hysteretic behavior of a TTBRB.

**Keywords:** buckling restrained brace; circumference pre-stress; interference fit; hysteretic behavior; design method

## 1. Introduction

The Buckling Restrained Brace (BRB) can yield under cycle loads when the structure is under seismic attacked, and thus dissipates the seismic energy. A typical BRB is composed of an internal steel core plate, an external restraining tube and de-bonding material between the core plate and the external restraining tube. The de-bonding material usually is made by concrete like material which has a low tensile strength whose fracture can greatly degrade the hysteretic behavior of a BRB.

Judd *et al*. (2016) carried out cyclic tests on an all-steel web-restrained-brace to investigate its hysteretic behavior under the combined axial and rotational load. Three different sizes of steel core plates were examined. All specimens successfully completed the cyclic testing up to 2% story drift without experiencing the brace instability failure, the brace end connection failure, or the rupture failure. Speicher and Harris (2018) presented the seismic performance of six special concentrically braced frames following requirements of ASCE 41-06. Recommendations were made on how to alter the frame performance, such as using alternative ground motion selection approaches, employing acceptance criteria based on cumulative ductility demand or energy dissipation. Atlayan and Charney (2014) introduced a new hybrid buckling-restrained braced. The hybrid term for the BRB system came from the use of different steel materials, including carbon steel, high-performance steel and low yield point steel in the core of the brace.

Guerrero *et al*. (2018) conducted shaking table tests on two four-story frames at a scale of 1/3 to examine the effects of BRBs on precast, reinforced concrete frames. The most significant finding of this study was that, for the linear-elastic response, the BRBs increased the damping ratio of the frame significantly. Retrofitting was also explored by replacing BRBs in Model 2 after the original model subjected to the seismic tests. Momenzadeh *et al*. (2017) investigated an all-steel buckling-controlled brace with two different configurations and compared its behavior with the conventional brace in terms of energy dissipation and ductility capacities. The BRB with round-in-square tube section had stable hysteretic behavior either when thickness ratio of the outer tube to inner tube was greater than 1.0 or when an enhanced gusset plate was employed. Heidary-Torkamani and Maalek (2017) carried out a comprehensive parametric investigation on the Tube-in-Tube Buckling Restrained Brace (TiTBRB) under cyclic loads through detailed Finite Element Model (FEM) analysis accounting for material and geometric nonlinearities as well as the effects of gaps and contacts. FEM analysis results

*Corresponding author, Ph.D., Professor,
E-mail: pjwang@sdu.edu.cn
**Co-corresponding author, B.E. Senior Engineer,
E-mail: sqhu@cztss.com



ISSN: 1229-9367 (Print), 1598-6233 (Online)

demonstrated that the proposed TiTBRB - if well designed - would not be failed by local or global buckling. Ozcelik *et al*. (2017) presented test results on BRBs with new end restraints and casing members. The innovation of their study was that additional end restraints were added at the unrestrained part. The isolation material was also employed between the core member and the restraining member. Test results indicated that the new BRB could undergo up to elongation rate of 2.0%.

Mirtaheri *et al*. (2017) presented FEM analysis results on BRBs without the filler material. Analysis results indicated that the flexural stiffness of restraining member, regardless of the amount of empty space, significantly affected the brace Global Buckling (GB) behavior. Kim and Choi (2015) suggested reinforcing H-shaped braces with non-welded cold-formed stiffeners to restrain the flexure failure and the buckling failure, and help to resist the tensile force and the compressive force equally. Analysis results showed that the proposed BRB satisfied the AISC requirement. Ghowsi and Sahoo (2015) presented an analytical investigation on the seismic response of a medium-rise BRB braced frame under the near-fault ground motions. Main parameters evaluated were the inter-story and residual drift response, the brace ductility, and the plastic hinge mechanisms. Piedrafita *et al*. (2015) presented a new BRB consisted of a perforated core plate which was guided and partially stabilized by the restraining unit. This design enabled the yielding force and plastic deformation of the BRB to be adjusted through changing the modular types. Chou *et al*. (2016) carried out a series of cyclic tests to study the behavior of large-scale dual-core self-centering braces and sandwiched BRBs. Hoveidae *et al*. (2015) presented a short core BRB which could be easily fabricated, inspected, and replaced after a severe earthquake. For a given story drift, the short core could develop bigger axial strain, compared with a full core BRB. Chen *et al*. (2016) tested seven all-steel BRBs under cyclic load to investigate effects of the de-bonding material on the performance of BRBs. The de-bonding material was made of 1mm thick Butyl Rubber or pure air gap between the core plate and the restraining system. Test results indicated that all the BRBs exhibited well energy dissipation capacities and sustained cumulative plastic deformations over 1000 times the yield strain. Hosseinzadeh and Mohebi (2016) proved advantages of the all steel BRB through using it in the representative truss elements to retrofit three 4-, 8-, and 12-story frames.

The design method for BRBs was first proposed by Takahashi and Mochizuki (1979). The core was determined by the axial force obtained from the structure analysis considering the seismic action. The restraining component should be designed to ensure that the BRB did not buckle before the core plate yielding. To satisfy this requirement, the restraining ratio $\xi$ should satisfy

$$\xi = \frac{P_{cr}}{P_y} \geq 1 \tag{1}$$

where $P_{cr}$ was the Euler buckling strength of the BRB system; and $P_y$ was the yield strength of the core plate.

Contact forces between the core and the restraining member are a key factor to determine the behavior of a BRB. Sutcu *et al*. (2014) evaluated the damage distribution and self-centering functions of BRBs connected to RC frames. A simplified method was proposed based on equivalent linearization to design the required amount of BRBs for retrofitting existing RC buildings.

Compared with BRB with concrete like de-bonding material, all-steel BRBs have more advantages. Tremblay *et al*. (2006) carried a series of tests to investigate the hysteretic behavior of BRBs under cyclic loads. Zhang *et al*. (2016) proposed a similar type BRB comprising three circular steel tubes with different diameters. Slotted holes were arranged on the core tube. The inner and outer tubes provided restraint to the core tub. The axial strength of the brace could be effectively adjusted through introducing slot holes to the core tube. However, the large hole ratio also caused significant stress concentration at the hole ends. For specimen B3 and B4, the tension fracture occurred at the end of the slotted holes under the loading amplitude of l/100. The early fracture of the core tube cannot be accepted for seismic energy dissipation device. At the same time, the slots reduced the local buckling strength of core tube. Moreover, no circumference stress could be generated in the core tube due to the existence of the slots.

This paper presents a Three-Tube Buckling-Restrained Brace (TTBRB), which is composed of one core tube in the middle and two restraining tubes outside and inside the core tube, as shown in Fig. 1. The core tube consists of two non-yielding parts at the two ends and one yielding part in the middle.

The two restraining tubes in the TTBRB can provide restraint to both global buckling and local buckling of the core tube. Compared with a solid section, the tube has a great radius-to-thickness ratio to make full use of the bending stiffness of the core. The outer and inner tubes restrain the deformation of the core tube in radius direction, which causes circumference stress ($\sigma_\theta$) in the core tube. Together with the circumference pre-Stress ($\sigma_{\theta,pre}$) in the core tube that is applied through hot fit of the outside tube or pre-tension stress through cold fit of the inside tube, the yield strength of core tube in axial direction ($\sigma_z$) can be improved. Ultra-High Molecular Weight Poly-Ethylene (UHMWPE) tubes with thickness of 0.2mm are installed between the tubes to reduce the friction when the core tube was axially elongated or shortened. One-sided bolts at the end of the TTBRB works as stoppers to maintain the relative positions of the three tubes.

Based on the fringe fiber yield criteria, the design method for the two restraining tubes is proposed. Parameter studies using verified Finite Element Model (FEM) are carried out to show the validation of the proposed method. The gap between the core tube and restraining tubes exists inevitably due to the manufacturing tolerance. Effects of gap width and $\sigma_{\theta,pre}$ on the behavior of the TTBRB are investigated using the verified FEM.

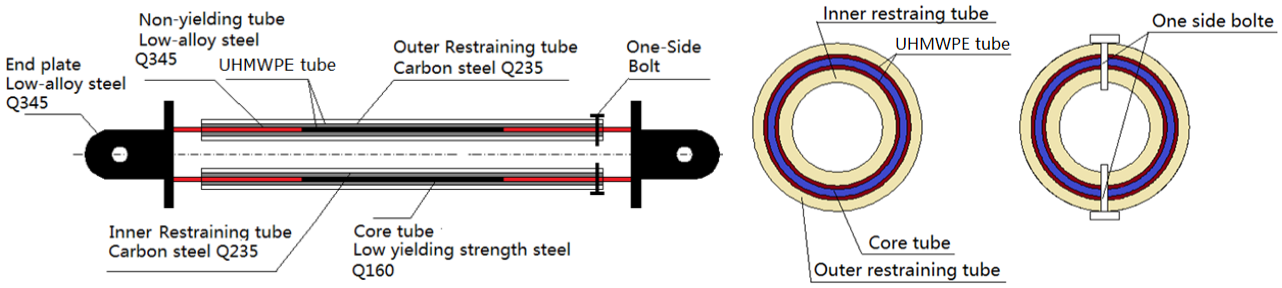


Fig. 1 Configuration of TTBRB

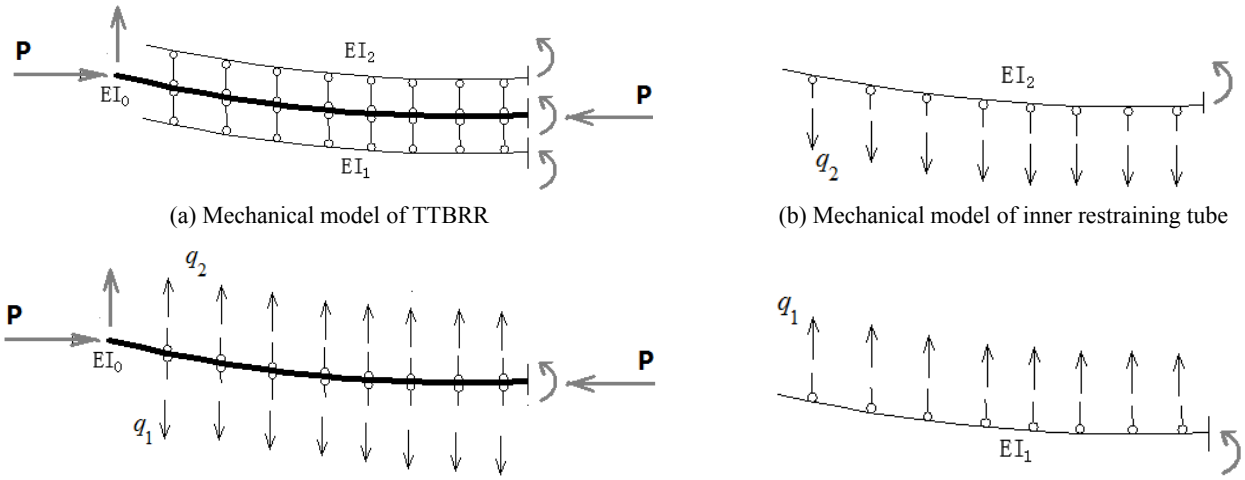


(a) Mechanical model of TTBRR

(b) Mechanical model of inner restraining tube

(c) Mechanical model of core tube

(d) Mechanical model of outer restraining tube

Fig. 2 Mechanical model of TTBRB under axial load

## 2. Design method for restraining tubes of TTBRB

Assume the outer and inner restraining tubes are tightly contact with the core tube, which means that there is no separation between them. The local buckling of the core tube can be efficiently prevented. On the other hand, the local buckling of the restraining tubes is avoided through choosing a proper radius-to-thickness ratio.

The mechanical model of a hinge-ended TTBRB under axial load is illustrated in Fig. 2. Only half of the model is studied for the symmetry of the model. $I_1$, $I_2$, $I_0$ represents the moment of inertia of the outer restraining tube, the inner restraining tube and the core tube, respectively. l is the total length of the TTBRB and $A_0$ is the cross-section area of the core tube. z represents the axial coordinate measured from the left end. $w_0$ is the initial middle span deflection of the BRB and w is the deflection of the BRB under axial load. $a_0$ is the initial geometric imperfection of the BRB at the middle span.

Before the yielding of the core tube, the bending moment equilibrium equation of the deflected core tube is

$$EI_0 w'' + P\cdot(w+w_0) = -\int_0^z [q_1(t)+q_2(t)](z-t)dt \tag{2}$$

where $q_1(t)$ and $q_2(t)$ are the distributed supporting forces provided by the outer and inner restraining tubes, respectively.

The bending moment equilibrium equation of the outer restraining tube is

$$EI_1 w'' = \int_0^z q_1(t)(z-t)dt \tag{3}$$

and that of the inner restraining tube is

$$EI_2 w'' = \int_0^z q_2(t)(z-t)dt \tag{4}$$

Substitute Eqs. (3)-(4) into Eq. (2). The bending moment equilibrium of the core tube can be formulated as

$$E(I_0+I_1+I_2)w''+P\cdot(w+w_0)=0 \tag{5}$$

The deflection of the core tube is

$$w+w_0 = \frac{a_0}{1-P/P_{cr}}\sin(\pi z/L) \tag{6}$$

where $P_{cr}$ is the Euler load of the TTBRB

$$P_{cr} = \frac{\pi^2 E(I_0+I_1+I_2)}{l^2} \tag{7}$$

The initial geometric imperfection adopts

$$w_0 = a_0 \sin(\frac{\pi z}{l}) \tag{8}$$

Hence, the deflection of the core tube due to axial load is

$$w = \frac{a_0}{P_{cr}/P - 1} \sin(\pi z / L) \tag{9}$$

For there is no separation between the core tube and the two restraining tubes. The restraining tubes will have the same deflection with that of the core tube.

The core tube should totally yield to dissipate the seismic energy. The applied axial force $P$ equals to the yield strength of the core tube

$$P = P_y = f_y A_0 \tag{10}$$

The stiffness of the core tube should be ignored when it yields. Then the Euler buckling strength of the TTBRB is calculated by

$$P_{cr} = \frac{\pi^2 E(I_1 + I_2)}{l^2} \tag{11}$$

Assume

$$I_1 = I_2 \tag{12}$$

Then, the Euler buckling strength of the TTBRB is calculated by

$$P_{cr} = \frac{2\pi^2 E I_1}{l^2} \tag{13}$$

The distributed lateral forces provided by the outer and inner restraining tubes to the core tube are

$$q_1(z) = EI_1 w^{(4)} = \frac{\pi^4 E I_1 a_0}{l^4 (P_{cr}/P_y - 1)} \sin\frac{\pi z}{l} \tag{14}$$

$$P_{cr} = \frac{\pi^2 E\left(I_0 + I_1 + I_2\right)}{l^2} \tag{15}$$

The bending moment of outside restraining tube at position $z$ is

$$M_1(z) = EI_1 w'' = \frac{\pi^2 E I_1 a_0}{l^2 (P_{cr}/P_y - 1)} \sin\frac{\pi z}{l} \tag{16}$$

At the middle span, z = $l$/2, $M_1$ can be simplified as

$$M_1 = \frac{\pi^2 E I_1 a_0}{l^2 (P_{cr}/P_y - 1)} \tag{17}$$

The outer tube should be kept in elastic state to ensure that it provides enough restraining stiffness. Based on fringe fiber yielding criteria, the bending moment $M_1$ should satisfy

$$\frac{M_1}{W_1} < f_y \tag{18}$$

where

$$W_1 = I_1 / r \tag{19}$$

and $r$ is the radius of the outside tube.

Substitute Eqs. (17) and (19) into Eq. (18), the condition to keep the outer tube in elastic state is

$$P_{cr}/P_y > 1 + \frac{\pi^2 E a_0 r}{l^2 f_y} \tag{20a}$$

The overall buckling of the TTBRB will not occur if the radius of outside restraining tube $r$ satisfies Eq. (20a).

For simplicity, define the factor restraining factor, $\eta$, as

$$\eta = 1 + \frac{\pi^2 E a_0 r}{l^2 f_y} \tag{21}$$

The Eq. (20a) could be rewritten as

$$P_{cr} > \eta P_y \tag{20b}$$

## 3. Finite element model and verification

### *3.1 Finite element model*

The three tubes in a TTBRB are modeled using C3D8R in ABAQUS, a 3D 8-node linear brick elements with reduced integration. The core tube is made of Q160 steel with yield strength of 160 MPa. Two restraining tubes are made of Q235 with yield strength of 235 Mpa. The Young modulus and Poisson ratio of Q160 an Q235 steel to make the core tube and the two restraining tubs are 205 GPa and 0.3, respectively. Automatic stabilization technique is adopted to help the convergence of FEM simulation with the artificial damping coefficient of $2.0\times0^{-5}$ as results of parameter sensitive analysis. The local buckling of the core tube can be effectively restrained by the restraining tubes. Only the global geometric imperfection is included. Initial geometric imperfection with magnitude of 9 mm ($l$/1000) is introduced in all FEMs. On the circumference direction, there are 20 elements; and there are 4 elements on the tube thickness to reduce hourglass effects caused by reduced integration type elements.

For the symmetry of the problem, only a quarter of the TTBRB is modeled, as shown in Fig. 3. At the left end of the model, the Multi-Point Constraint (MPC) using the Beam option is applied to the core tube to simulate the pinned end boundary condition. The MPC control point is

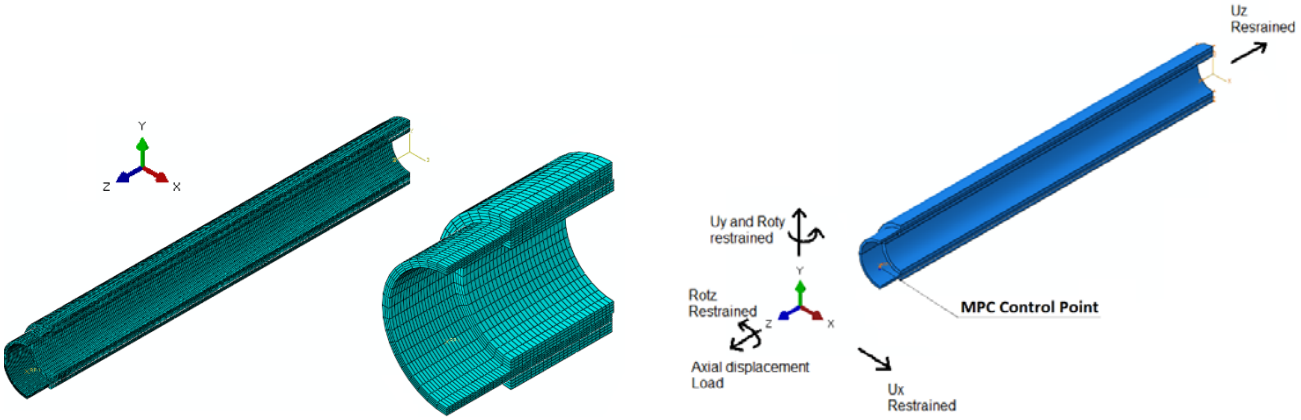


(a) Mesh of TTBRB (b) Boundary conditions

Fig. 3 Finite element model

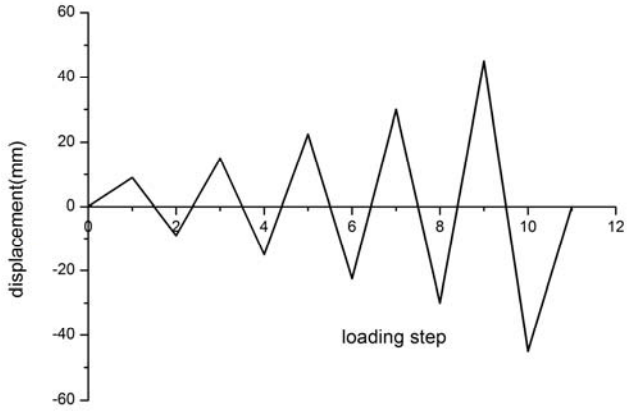


Fig. 4 Loading scheme

located at the center of three tubes. The $U_x$, $U_y$, $Rot_y$ and $Rot_z$ of the MPC control point are restrained. The $U_z$ is left to apply the axial displacement. Left ends of the two restraining tubes are free. The *xy*-plane symmetry boundary condition is applied to the right end of the core tube and the two restraining tubes, which is modelled through fixing the $U_z$. The contact properties between the core tube and the two restraining tubes are assumed to be hard contact on the normal direction and frictionless on the tangent direction owing to the UHMWPE layer.

For the manufacture tolerance, there might be a gap between the core tube and the restraining tubes, which is usually less than 2.0 mm. Effects of the gap on the behavior of a TTBRB are studied. UHMWPE tubes between the core tube and the two restraining tubes are ignored in the FEM for they do not provide lateral stiffness to the TTBRB.

The total length of the BRB, $l$, is assumed to be 9000 mm. Cyclic axial displacements are imposed at the one end of TTBRB with magnitude of $\pm l/500$, $\pm l/300$, $\pm l/200$, $\pm l/150$ and $\pm l/100$, as shown in Fig. 4.

### *3.2 Model verification*

#### *3.2.1 Verification by tests carried out by Tremblay et al. (2006)*

Tremblay *et al*. (2006) carried out seismic tests on six BRBs. Test results on S1-2 were selected to verify the proposed FEM. The core plate was sandwiched between two steel tube-guide plate assemblies that were bolted together. Cross-sectional dimensions of the core segment were 12.7 mm×125 mm ($A_c$ = 1588 mm$^2$), and the brace yield load, $P_y$, was 587 kN. The buckling of the brace core was prevented by a pair of ASTM A500 HSS 127×127×4.8 tubes, each being shop-welded to a 10 mm×270 mm guide plate. The brace core were inserted between the two guide plates, together with 12.7 mm filler plates and 0.8 mm shim plates, and all components were secured by bolts at a regular spacing.

Core plates were made of G40.21-350WT steel with nominal yield strength $f_y$ = 350 MPa and tensile stress $f_u$ = 450 MPa. The corresponding measured values from coupon tensile tests were 370 MPa and 492 Mpa, respectively. The deformation measured at the onset of strain hardening, $\varepsilon_{sh}$, was 1.9%, and the strain at fracture, $\varepsilon_{su}$, was 26.8%. Measured values of steel strength were used in the FEM.

For the existence of 0.8 mm shim plate, the gap width between core plate and guide plate was 0.8 mm, and there was no circumference stress in the core plate.

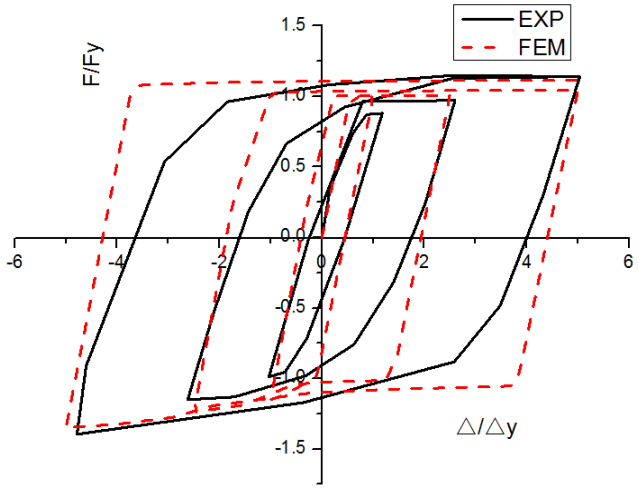


Fig. 5 Hysteretic curves of S1-2 obtained from test and FEM simulation

Hysteretic curves of S1-2 obtained from the seismic test and the FEM simulation are shown in Fig. 5. In the first quadrant and third quadrant in which the BRB is in tension and compression, respectively, hysteretic curves obtained from FEM almost coincide with experiment results. However, in the second and fourth quadrant, the curves obtained from FEM change sharply compared with those from tests, which might be caused by the constitute model in FEM was assumed to be elastic perfect plastic.

#### 3.2.2 Verification by tests carried out by Zhang et al. (2016)

Zhang *et al*. (2016) proposed a new type of BRB comprising three circular steel tubes with different diameters. Slotted holes were arranged on the core tube, whose out-of-plane deformation was restrained by the inner and outer restraining tubes. Test results on B2 were used to verify the FEM model.

Dimensions of the inner, middle and outer tubes were 2900 mm×140 mm×6 mm, 3000 mm×159 mm×8 mm and 1430 mm×180 mm×9 mm, respectively. The gap between the inner and the middle tubes and that between the middle and the outer tubers were both 1.5 mm, and no un-bonded material between the tubes. The length and width of the slotted hole of specimen B2 was 1300 mm 50 mm, respectively. All the steel tubes were made of Q235 steel. A coupon test revealed that the yield strength $f_y$ was 422 Mpa, ultimate strength $f_u$ of 639 MPa, and elongation ratio of 20%.

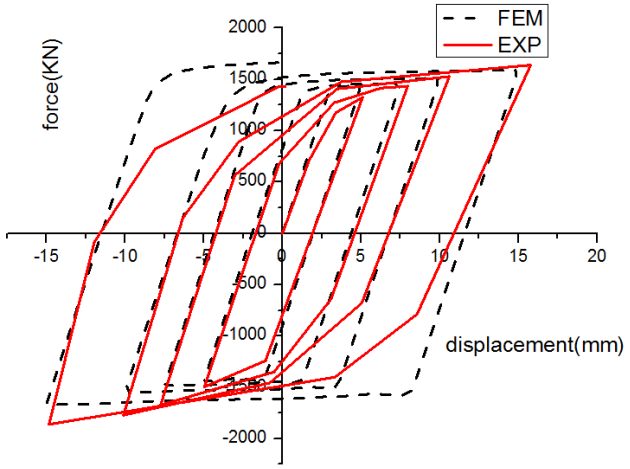


Fig. 6 Hysteretic curves of B2 obtained from test and FEM simulation

For the existence of 1.5 mm gap width between the core tube and the restraining tubes and the slot holes on the core tube of B2, no circumference stress would be induced in the core tube.

Hysteretic curves of B2 obtained from test and FEM simulation are shown in Fig. 6. In the second and fourth quadrant, the curves obtained from FEM change sharply compared with those from tests, which is due to the constitute model in FEM being different to the realistic steel model. However, in the first quadrant and third quadrant in which the BRB is in tension and compression, respectively, hysteretic curves obtained from FEM are almost the same with the experiment results, which shows the applicability of the FEM for predicting the behavior of TTBRBs.

## 4. Verification of proposed design equations for restraining tubes

Theoretically, if the restraint ratio satisfies the requirement of Eq. (20), the TTBRB would not encounter global flexure buckling. However, a TTBRB could have different radius-thickness ratio for a given axial strength. Hence, the requirement for the restraining tubes could be changed. At the same time, gaps between tubes exist inevitably due to the manufacture tolerance. $\sigma_{\theta,pre}$ could also be introduced to the core tube. It should be verified whether the Eq. (20) is applicable for a TTBRB with different radius-thickness ratios, with different gap widths between core tube and restraining tubes, and with different levels of $\sigma_{\theta,pre}$.

### 4.1 TTBRBs with core tubs with different radius-to-thickness ratios

Four core tubes with different radius-to-thickness ratios are selected, which are 150 mm×15 mm, 200 mm×10 mm, 250 mm×8 mm and 400 mm× 5 mm. The corresponding thicknesses of outer and inner restraining tubes calculated by Eq. (20) are 14.1 mm, 6.33 mm, 3.46 mm and 0.93 mm, respectively, as listed in Tables 1-4. The length of the TTBRB is 9000 mm. $t_1$ and $t_2$ are the thickness of outside and inside restraining tubes, respectively. $a_1$ and $a_2$ are the gap width between the core-outer restraining tube and the core-inner restraining tube, respectively.

From Tables 1-4, it can be seen that the TTBRB

Table 1 TTBRBs with core tube of 150×15

| Model No. | $t_1$ & $t_2$ calculated by Eqs. (20) and (21) (mm) | $t_1$ & $t_2$ adopted in FEM (mm) | $\zeta = P_{cr}/P_y$ | $a_1$ (mm) | $a_2$ (mm) | $\eta$ calculated by Eq. (21) | $\alpha = \zeta/\eta$ | Failure mode |
|---|---|---|---|---|---|---|---|---|
| P-1 | 14.1 | 15 | 1.06 | 0 | 0 | 1.233 | 0.88 | GB |
| P-2 | 14.1 | 18 | 1.28 | 0 | 0 | 1.237 | 1.06 | GB |
| P-3 | 14.1 | 20 | 1.41 | 0 | 0 | 1.240 | 1.175 | GB |
| P-4 | 14.1 | 22 | 1.63 | 0 | 0 | 1.243 | 1.35 | GB |
| **P-5** | **14.1** | **23** | **1.92** | **0** | **0** | 1.244 | **1.60** | **SY** |
| **P-6** | **14.1** | **25** | **2.12** | **0** | **0** | 1.247 | **1.76** | **SY** |

Table 2 TTBRBs with core tube of 200×10

| Model No. | $t_1$ & $t_2$ calculated by Eqs. (20) and (21) (mm) | $t_1$ & $t_2$ adopted in FEM (mm) | $\zeta = P_{cr}/P_y$ | $a_1$ (mm) | $a_2$ (mm) | $\eta$ calculated by Eq. (21) | $\alpha = \zeta/\eta$ | Failure mode |
|---|---|---|---|---|---|---|---|---|
| X-1 | 6.33 | 5 | 0.87 | 0 | 0 | 1.289 | 0.78 | GB |
| X-2 | 6.33 | 6 | 1.05 | 0 | 0 | 1.291 | 0.94 | GB |
| X-3 | 6.33 | 7 | 1.22 | 0 | 0 | 1.292 | 1.09 | GB |
| X-4 | 6.33 | 8 | 1.41 | 0 | 0 | 1.293 | 1.27 | GB |
| **X-5** | **6.33** | **9** | **1.59** | **0** | **0** | **1.295** | **1.43** | **SY** |
| **X-6** | **6.63** | **10** | **1.77** | **0** | **0** | **1.296** | **1.59** | **SY** |

Table 3 TTBRBs with core tube of 250×8

| Model No. | $t_1$ & $t_2$ calculated by Eqs. (20) and (21) (mm) | $t_1$ & $t_2$ adopted in FEM (mm) | $\zeta = P_{cr}/P_y$ | $a_1$ (mm) | $a_2$ (mm) | $\eta$ calculated by Eq. (21) | $\alpha = \zeta/\eta$ | Failure mode |
|---|---|---|---|---|---|---|---|---|
| K-1 | 3.46 | 2 | 0.65 | 0 | 0 | 1.355 | 0.59 | GB |
| K-2 | 3.46 | 3 | 0.97 | 0 | 0 | 1.357 | 0.85 | GB |
| K-3 | 3.46 | 4 | 1.31 | 0 | 0 | e | 1.15 | GB |
| **K-4** | **3.46** | **5** | **1.63** | **0** | **0** | **1.360** | **1.44** | **SY** |
| **K-5** | **3.46** | **6** | **1.96** | **0** | **0** | **1.361** | **1.73** | **SY** |

Table 4 TTBRBs with core tube of 400×5

| Model No. | $t_1$ & $t_2$ calculated by Eqs. (20) and (21) (mm) | $t_1$ & $t_2$ adopted in FEM (mm) | $\zeta = P_{cr}/P_y$ | $a_1$ (mm) | $a_2$ (mm) | $\eta$ calculated by Eq. (21) | $\alpha = \zeta/\eta$ | Failure mode |
|---|---|---|---|---|---|---|---|---|
| O-1 | 0.93 | 0.8 | 1.02 | 0 | 0 | 1.565 | 0.85 | GB |
| O-2 | 0.93 | 1.0 | 1.28 | 0 | 0 | 1.566 | 1.06 | GB |
| O-3 | 0.93 | 1.5 | 1.92 | 0 | 0 | 1.566 | 1.60 | GB |
| O-4 | 0.93 | 1.6 | 2.17 | 0 | 0 | 1.566 | 1.72 | GB |
| **O-5** | **0.93** | **1.7** | **2.17** | **0** | **0** | **1.567** | **1.80** | **SY** |
| **O-6** | **0.93** | **1.8** | **2.30** | **0** | **0** | **1.567** | **1.92** | **SY** |

encounters Global Buckling (GB) when the thickness of restraining tubes takes $\eta$ calculated by Eq. (21). To ensure the Section Yielding (SY) of the core tube, the $\eta$ should be increased by a factor $\alpha$ at least of 1.80, as listed in Tables 1-4. To provide a conservative design, here a factor of 2.0 is proposed

$$\eta_m = 2.0\eta \tag{22}$$

in which $\eta_m$ is the modified restraining factor. The Eq. (20) should be rewritten as

$$P_{cr} > \eta_m P_y \tag{20b}$$

The load-displacement curves of TTBRBs in Group X with different restraining tube thickness are illustrated in Fig. 7. The middle span displacements of X-4, X-5 and X-6 are shown in Fig. 8. It could be seen that the restraining tubes could effectively prevent the GB failure of a TTBRB if the restraining tube is designed according to Eq. (20b).

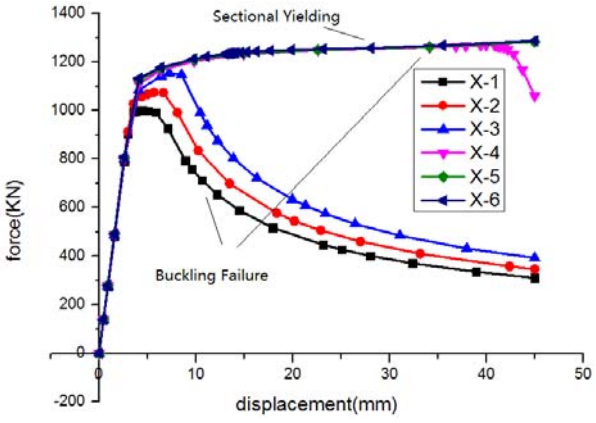


Fig. 7 Load-displacement curves of TTBRBs in Group X

The development of $\sigma_\theta$ and $\sigma_z$ of the outer tube are shown in Fig. 9. The existence of $\sigma_\theta$ in outer restraining tube is caused by the expansion of the core tube in radius

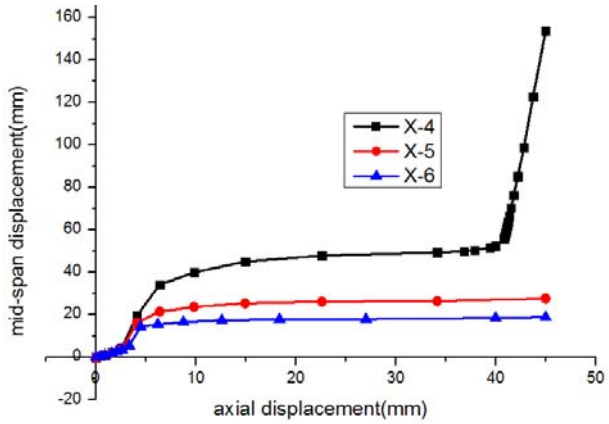


Fig. 8 Mid-span displacement of TTBRBs in Group X

direction. It keeps increasing with the increase of axial force, as shown in Fig. 9(a). For a TTBRB failed by GB failure mode, the longitudinal stress $\sigma_z$ in the outside tube is far less than the yield strength, as shown in Fig. 9(b).

The axial stress distribution of the three tubes in TTBRB X-3 and X-6 clearly reflects their failure modes, as shown in Fig. 10. The stress gradient in Model X-3 indicates that it is failed by GB failure; and the uniform stress distribution in X-5 indicates that it is failed by SY failure.

It can be concluded that the radius to thickness ratio of the core tube has no influences on the failure mode of the TTBRB if the restraining tube is designed according to Eq. (20b).

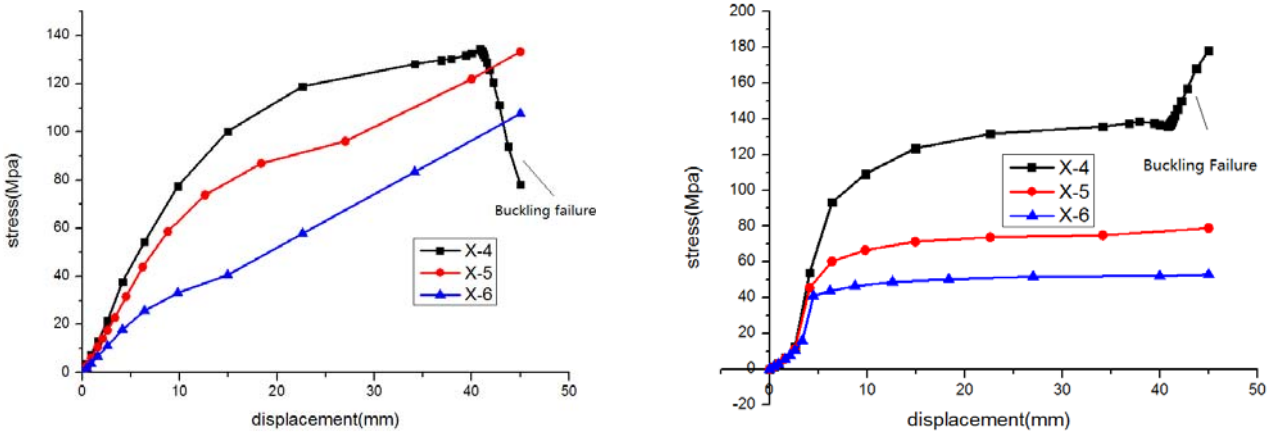


(a) Circumference stress in outer restraining tube

(b) Axial stress in outer restraining tube

Fig. 9 Circumference and axial stresses in outer tub

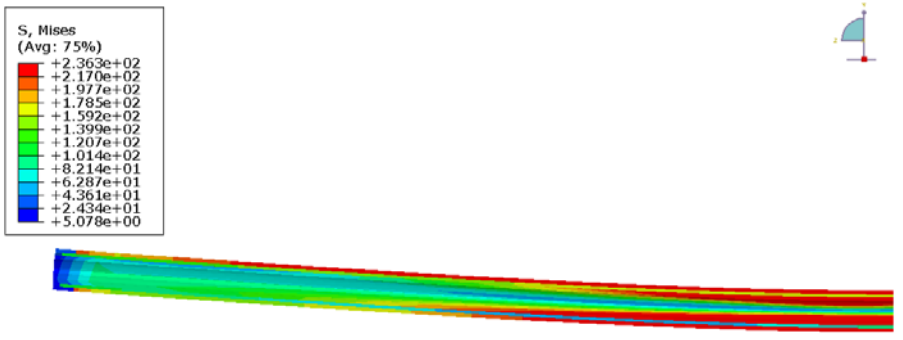


(a) Global buckling of X-3

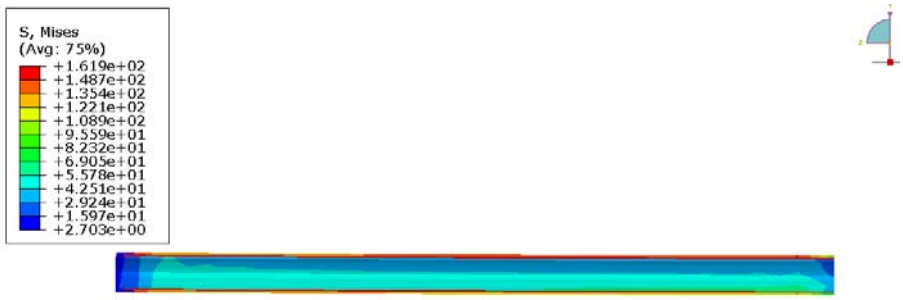


(b) Sectional yielding of X-6

Fig. 10 Axial stresses distribution of the three tubes in a TTBRB

Table 5 TTBRBs with core tube of 200×10 for investigating effects of gap width

| Model No. | $t_1$ & $t_2$ calculated by Eqs.(20) and (22) (mm) | $t_1$ & $t_2$ adopted in FEM (mm) | $\zeta = P_{cr}/P_y$ | $a_1$ (mm) | $a_2$ (mm) | Failure mode |
|---|---|---|---|---|---|---|
| T1-0 | 12.6 | 13 | 2.32 | 0 | 0 | SY |
| T1-1 | 12.6 | 13 | 2.32 | 0.5 | 0 | SY |
| T1-2 | 12.6 | 13 | 2.32 | 0 | 0.5 | SY |
| T1-3 | 12.6 | 13 | 2.32 | 0.5 | 0.5 | SY |
| T2-0 | 12.6 | 13 | 2.32 | 0 | 0 | SY |
| T2-1 | 12.6 | 13 | 2.40 | 2.0 | 0 | SY |
| T2-2 | 12.6 | 13 | 2.27 | 0 | 2.0 | SY |
| T2-3 | 12.6 | 13 | 2.35 | 2.0 | 2.0 | SY |
| T3-0 | 12.6 | 13 | 2.32 | 0 | 0 | SY |
| T3-1 | 12.6 | 13 | 2.52 | 5.0 | 0 | SY |
| T3-2 | 12.6 | 13 | 2.21 | 0 | 5.0 | SY |
| T3-3 | 12.6 | 13 | 2.41 | 5.0 | 5.0 | SY |

### *4.2 TTBRBs with different gap widths between tubes*

The derivation of Eq. (20b) does not consider the influence of the gap between the core and restraining tubes. Studied TTBRBs with gaps are listed in Table 5. The length of TTBRB is 9000 mm. The gap width between the core and the restraining tubes could be caused be manufacture tolerance, which is usually less than 2.0 mm.

From Table 5, it can be seen that the TTBRBs are all failed by SY failure if the radius of outer restraining tube satisfies the Eq. (20b), no matter it has or has no gap

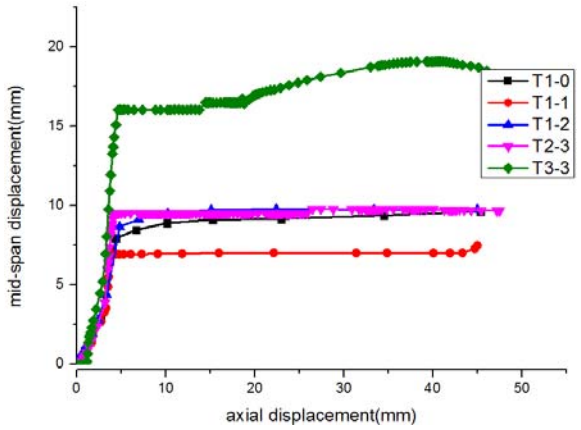


(a) Mid-span displacement of core tube

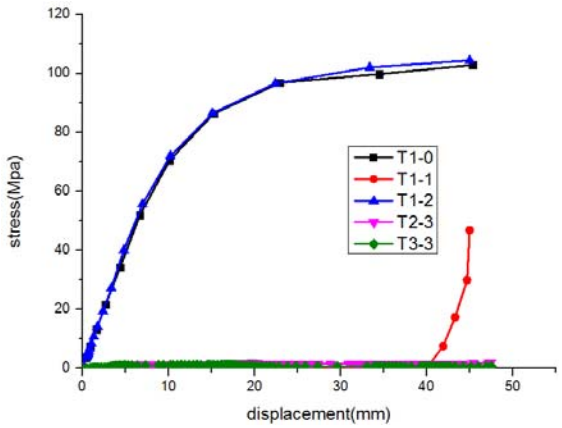


(b) Circumference stress of outer tube at mid-span section

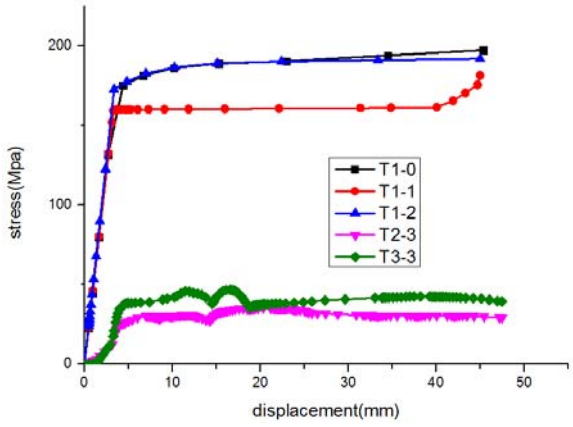


(c) Axial stress of outer tube at the tensile side of mid-span section

Fig. 11 Stress and displacement of TTBRBs with gap between core and restraining tubes

Table 6 TTBRBs with core tube of 200×10 for investigating effects of pre-stress

| Model No. | $t_1$ & $t_2$ calculated by Eq. (20) and (22) (mm) | $t_1$ & $t_2$ adopted in FEM (mm) | $\zeta = P_{cr}/P_y$ | Circumference stress (N/mm$^2$) | | | Failure mode |
|---|---|---|---|---|---|---|---|
| | | | | Outside tube | Core tube | Inside tube | |
| F1-0 | 12.6 | 13 | 2.32 | 0 | 0 | 0 | SY |
| F1-1 | 12.6 | 13 | 2.32 | 80 | -40 | -45 | SY |
| F1-2 | 12.6 | 13 | 2.32 | 120 | -55 | -65 | SY |
| F1-3 | 12.6 | 13 | 2.32 | 160 | -75 | -90 | SY |
| **F1-4** | **12.6** | **13** | **2.32** | **185** | **-90** | **-105** | **GB** |
| F2-1 | 12.6 | 13 | 2.32 | 60 | 70 | -100 | SY |
| F2-2 | 12.6 | 1e | 2.32 | 90 | 100 | -165 | SY |
| **F2-3** | **12.6** | **13** | **2.32** | **130** | **150** | **-225** | **GB** |
| F3-1 | 12.6 | 13 | 2.32 | 0 | 60 | -45 | SY |
| F3-2 | 12.6 | 13 | 2.32 | 0 | 95 | -70 | SY |
| F3-3 | 12.6 | 13 | 2.32 | 0 | 120 | -90 | SY |
| F3-4 | 12.6 | 13 | 2.32 | 0 | 150 | -115 | SY |

between the core and the restraining tubes.

It would not affect the middle span deflection of the core tube if the gap width is smaller than 2.0 mm, as shown in Fig. 11(a). For the TTBRB with a great gap width, the lateral displacement keeps increasing until the core tube contacts the restraining tubes. The development $\sigma_\theta$ and $\sigma_z$ in outer tube proves the contact between core tube and outer restraining tube. For the model T1-1, a small gap width of 0.5 mm can effectively release the $\sigma_\theta$ in the outside tube in the initial loading stage. With the load increasing, $\sigma_\theta$ in the outside tube increases sharply because the core tube is restrained by the outside tube after the contact between them. For the Model T1-0 and T1-2, the outer tube and the core tube are tightly contact for the gap width is 0. The $\sigma_\theta$ and $\sigma_z$ in outer tube of T1-0 and T1-2 increases from the beginning. For the T2-3 and T3-3, the gap width between the outer tube and the core tube are 2.0 mm and 5.0 mm, respectively. Hence, there is no $\sigma_\theta$ in the outer tube; and the $\sigma_z$ in outer tube starts to increase after they contact with each other, as shown in Figs. 11(b) and (c).

The development of mid-span displacement and stresses of T1-0 and model T1-2 are nearly the same, as shown in Figs. 11(a), 15(b) and 15(c), which indicates that the gap between core tube and inner tube does not affect the behavior of a TTBRB when it is in compression condition.

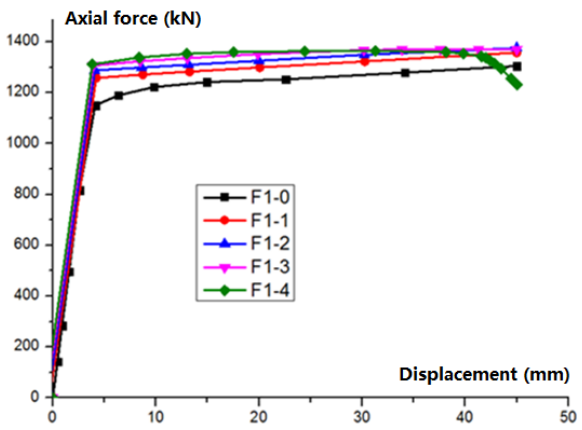


Fig. 12 Load-displacement curves of TTBRBs in Group F1

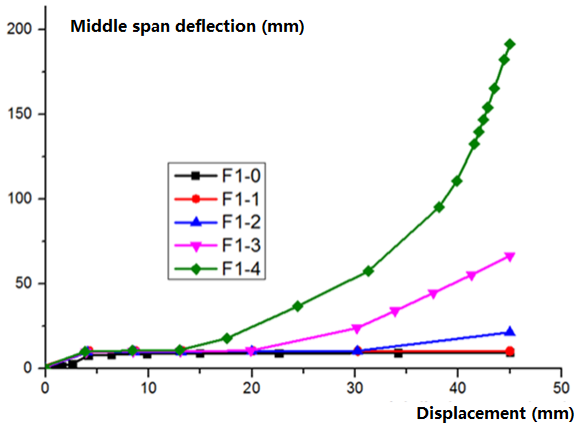


Fig. 13 Mid-span displacement of outer tube of TTBRBs in Group F1

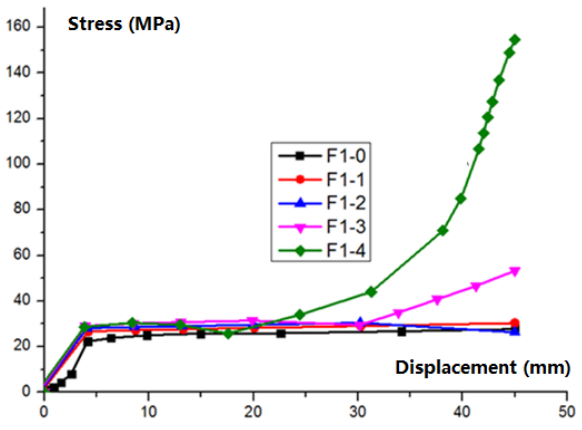


Fig. 14 Axial stress of outer tube at tensile side of mid-span of TTBRBs in Group F1

### *4.3 TTBRBs with different circumference pre-stresses*

The derivation of Eq. (20b) does not consider the influence of the circumference pre-stress, $\sigma_{\theta,pre}$, in the core tube. Through introducing $\sigma_{\theta,pre}$ to the core tube, its yield strength in the axial direction can be adjusted. The studied TTBRBs with different $\sigma_{\theta,pre}$ are listed in Table 6. The length of the studied TTBRB is 9000 mm. The compression $\sigma_{\theta,pre}$ in core tube in Group F1 is applied through hot fit of the outer tube. The tension $\sigma_{\theta,pre}$ in core tube in Group F2 and F3 is applied through cold fit of the inner tube. There is no tension $\sigma_{\theta,pre}$ in the outer tube in Group F3, fore the existence of gap with width of 0.1 mm between the core tube and the outer tube. They can be measured through strain gauges.

For the core tube with compression $\sigma_{\theta,pre}$ being greater than -75 MPa, the restraining tubes designed by Eq. (20b) are still effectively able to prevent the GB failure of the TTBRB, as listed in Table 6. Otherwise, thicker restraining tubes should be adopted to prevent the GB failure of a TTBRB.

Similarly, for the core tube with tension $\sigma_{\theta,pre}$ being lower than 100 MPa, the restraining tubes designed by Eq. (20b) are applicable, as listed in Table 6. If there is no tension $\sigma_{\theta,pre}$ in the outer restraining tube, the Eq. (20b) is still applicable for TTBRBs with tension $\sigma_{\theta,pre}$ being up to 150 MPa in the core tube, as listed in Table 6.

The load-displacement curves of TTBRBs in Group F1 clearly show that F1-F4 are failed by GB failure, as shown in Figs. 12 and 13. If the TTBRBs are failed by SY failure, the axial stress of outer tube at tensile side of middle span remains in a low level, as shown in Fig. 14. The circumference stress of outer tube at mid-span keeps increase from its initial value till it reaches the level of 200 MPa, as shown in Fig. 15.

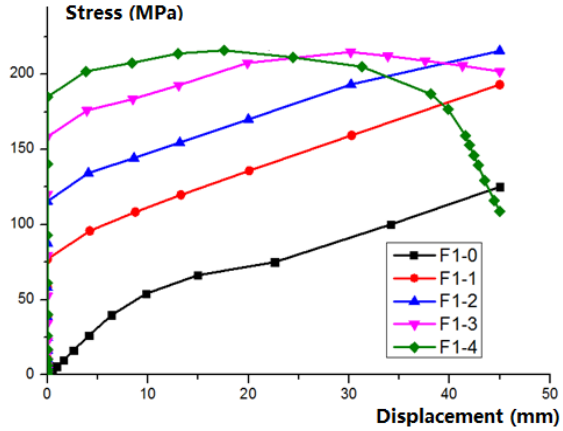


Fig. 15 Circumference stress of outer tube at mid-span of TTBRBs in Group F1

The circumference stress in the outer tube would reach the yield stress, for the existence of tension $\sigma_{\theta,pre}$. The flexural stiffness of the outer tube should be ignored when it yields. Eq. (13) should be revised as

$$P_{cr} = \frac{\pi^2 EI_1}{l^2} \tag{23}$$

That is, only the stiffness of inner restraining tube is considered. Then the radius of inner restraining tube could be determined through Eqs. (20b) and (23). Calculated results are listed in Table 7. It can be seen that the Eq. (20b) is still applicable for TTBRBs with circumference pre-stress in core tube, if the global buckling strength of a TTBRB is calculated by Eq. (23).

Whether the circumference pre-stress affects the proposed design equations depends on its magnitude. For the core tube with compression $\sigma_{\theta,pre}$ being greater than -75 MPa or with tension $\sigma_{\theta,pre}$ being lower than 100 MPa, the Eq. (20b) is still applicable. Otherwise, the Eq. (13) should be replaced by Eq. (23), then the restraining tubes are determined by Eq. (20b).

## 5. Constitute model of core tube in TTBRBs

The radius of the core tube would change following the Poisson's ratio under axial load. This changes are restrained by the outer and inner restraining tubes, which causes the existence of $\sigma_\theta$ and $\sigma_r$ in the three tubes, in turn. At the same time, the $\sigma_{\theta,pre}$ can also be applied to the core tube through interference fit of the outer or the inner restraining tube.

According the von Mises yielding criterion, the existence of circumference stress ($\sigma_\theta$) and radius stress ($\sigma_r$) would affect the strength in axial direction ($\sigma_z$)

$$\frac{1}{2}[(\sigma_z-\sigma_r)^2+(\sigma_z-\sigma_\theta)^2+(\sigma_r-\sigma_\theta)^2] \le \sigma_y^2 \tag{24}$$

The yield strength of the core tube with different $\sigma_{\theta,pre}$ in

Table 7 TTBRBs with core tube of 200×10 for validating Eq. (20b)

| Model No. | $t_1$ & $t_2$ calculated by Eqs. (23), (20) and (22) (mm) | $t_1$ & $t_2$ adopted in FEM (mm) | $\zeta = P_{cr}/P_y$ | Circumference stress (N/mm$^2$) | | | Failure mode |
|---|---|---|---|---|---|---|---|
| | | | | Outside tube | Core tube | Inside tube | |
| **F1-4** | **25.2** | **13** | **1.16** | **185** | **-90** | **-105** | **GB** |
| F1-4a | 25.2 | 26 | 1.65 | 181 | -90 | -104 | SY |
| F1-5 | 25.2 | 26 | 1.65 | 230 | -125 | -160 | SY |
| **F2-3** | **25.2** | **13** | **1.16** | **130** | **150** | **-225** | **GB** |
| F2-3a | 25.2 | 26 | 1.65 | 126 | 150 | -221 | SY |
| F2-4 | 25.2 | 26 | 1.65 | 145 | 160 | -200 | SY |

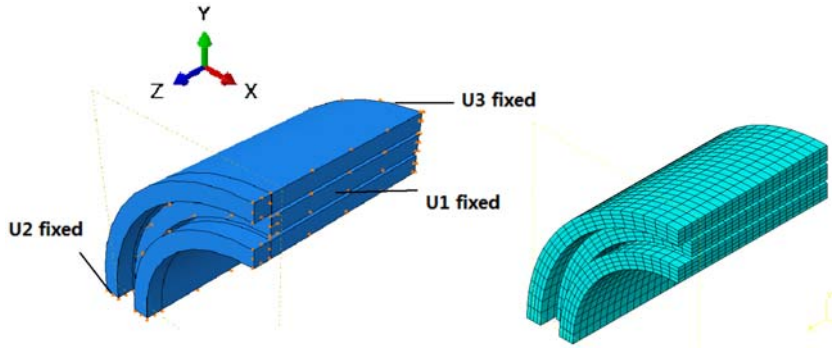


Fig. 16 Finite element model for investigating constitute model of core tub

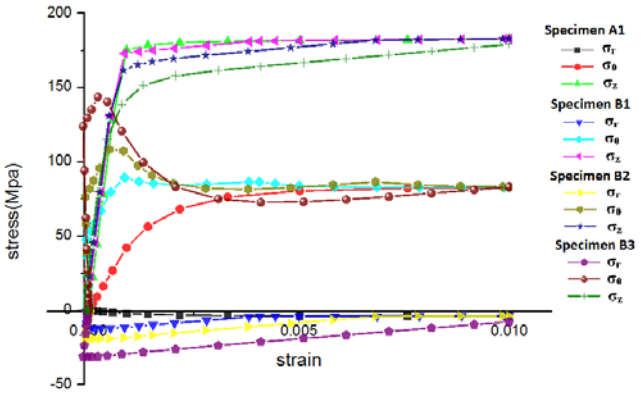


Fig. 17 Evolution of $\sigma_r$, $\sigma_\theta$, and $\sigma_z$ with increase of tension strain under different $\sigma_{\theta,pre}$

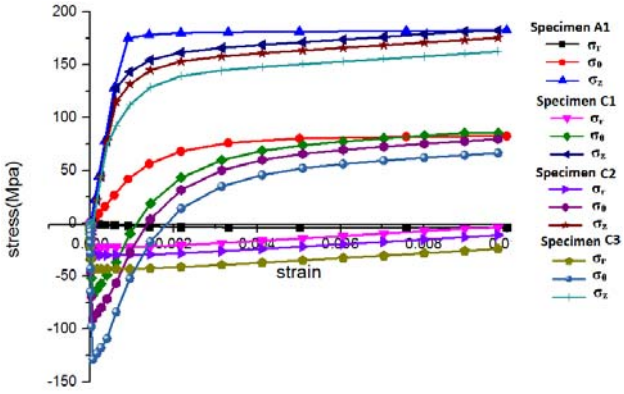


Fig. 18 Evolution of $\sigma_r$, $\sigma_\theta$, and $\sigma_z$ with increase of tension strain under different compression $\sigma_{\theta,pre}$

Table 8 Yield strength of core tube under tension with different tension $\sigma_{\theta,pre}$

| Model No. | $\sigma_{\theta,pre}$ (MPa) | Stresses at tension yielding | | | |
|---|---|---|---|---|---|
| | | $\sigma_\theta$ (MPa) | $\sigma_\theta/f_y$ | $\sigma_z$ (MPa) | $\sigma_z/f_y$ |
| A1 | 0 | 80 | 0.5 | 185 | 1.156 |
| B1 | 45 | 80 | 0.5 | 185 | 1.156 |
| B2 | 85 | 80 | 0.5 | 185 | 1.156 |
| B3 | 125 | 80 | 0.5 | 185 | 1.156 |

core tube is investigated using FEM simulation. The length of the model is selected to be 100 mm to ensure it is failed by SY failure. For the symmetry of the model, only a quarter is modelled, as shown in Fig. 16. The thickness of the core tubes is 10 mm; and those of the outer and inner tubes are 26 mm.

The model is meshed using C3D8R in ABAQUS. The core tube is made of steel Q160 with yield strength of 160 MPa. The two restraining tubes are made of Q235 with yield strength of 235 Mpa. The Young's modulus and Poisson ratio of steel to make the core tube and the two restraining tubs are 205 GPa and 0.3, respectively. Boundary conditions are also shown in Fig. 16.

### *5.1 Yield strength of core tube in tension*

When the core tube is in tension, the existence of inner tube will restrain the shrinkage of the core tube in radius direction, which causes tension $\sigma_\theta$. Together with the imposed $\sigma_{\theta,pre}$, the yield strength in axial can be adjusted.

Four levels of tension $\sigma_{\theta,pre}$ in the core tube are studied, as listed in Table 8. When the core tube yields in tension, no matter what level of $\sigma_{\theta,pre}$ is, the tension strength in $z$ direction is 185 MPa, which is about 1.156 times of $f_y$ and the $\sigma_\theta$ increases or reduces to 80 MPa, which is 0.5 times of $f_y$, as listed in Table 8 and shown in Fig. 17. Analysis results prove that the existence of inner tube causes circumference stresses in the core tube. Prior to the core tube encountering the GB and Local Buckling (LB) failure, the inner tube can also increase the tension strength of core tube by 1.156 times. Moreover, the bigger value of $\sigma_{\theta,pre}$ causes the core tube encounters the SY failure earlier. For example, the model B3 whose $\sigma_{\theta,pre}$ is 125 MPa yields at 120 Mpa in $z$ direction.

Four levels of compression $\sigma_{\theta,pre}$ in the core tube are studied, which are 0 MPa, -65 MPa, -90 MPa and -130 MPa, as listed in Table 9. When the core tube is in tension, the compression $\sigma_{\theta,pre}$ starts to decrease due to the development of the tension strain in circumference direction, as shown in Fig. 18.

When the compression $\sigma_{\theta,pre}$ is lower than -90 MPa, the ultimate tension strength in $z$ direction is 185 MPa, which is about 1.156 times of $f_y$ and the $\sigma_\theta$ is 80 MPa, which is 0.5 times of $f_y$. That is, effects of compression pre-stress in circumference direction are the same with those of the tension pre-stress.

Table 9 Yield strength of core tube under tension with different compression $\sigma_{\theta,pre}$

| Model No. | $\sigma_{\theta,pre}$ (MPa) | Stresses at tension yielding | | | |
|---|---|---|---|---|---|
| | | $\sigma_\theta$ (MPa) | $\sigma_\theta/f_y$ | $\sigma_z$ (MPa) | $\sigma_z/f_y$ |
| A1 | 0 | 80 | 0.5 | 185 | 1.156 |
| C1 | -65 | 80 | 0.5 | 185 | 1.156 |
| C2 | -90 | 80 | 0.5 | 185 | 1.156 |
| C3 | -130 | 70 | 0.438 | 150 | 0.938 |

Table 10 Yield strength of core tube under compression with different compression $\sigma_{\theta,pre}$

| Model No. | $\sigma_{\theta,pre}$ (MPa) | Stresses at tension yielding | | | |
|---|---|---|---|---|---|
| | | $\sigma_\theta$ (MPa) | $\sigma_\theta/f_y$ | $\sigma_z$ (MPa) | $\sigma_z/f_y$ |
| E1 | -65 | -135 | 0.844 | -230 | 1.438 |
| E2 | -90 | -135 | 0.844 | -235 | 1.469 |
| E3 | -125 | -135 | 0.844 | -235 | 1.469 |

When the compression $\sigma_{\theta,pre}$ is higher than -90 MPa, the tension strength in $z$ direction reduces to 150 MPa, which is about 0.938 times of $f_y$ and the $\sigma_\theta$ is 70 MPa, which is 0.438 times of $f_y$. That is, a high level of $\sigma_{\theta,pre}$ will affect the tension strength of the core tube.

### *5.2 Yield strength of core tube in compression*

When the core tube is in compression, the existence of outer tube restrains the expansion of the core tube in radius direction, which causes compression $\sigma_\theta$. Together with the imposed $\sigma_{\theta,pre}$, the yield strength in axial is improved.

Three levels of compression $\sigma_{\theta,pre}$ in the core tube are studied, which are -65 MPa, -90 MPa and -125 MPa. When the core tube yields in compression, the compression strength of the core tube in $z$ direction is higher than 230 MPa, which is about 1.438 times of $f_y$ and the compression $\sigma_\theta$ is about -135 MPa, which is 0.844 times of $f_y$, as listed in Table 10 and shown in Fig. 19. Compared to the tension strength of the core tube, the compression strength is greatly increased.

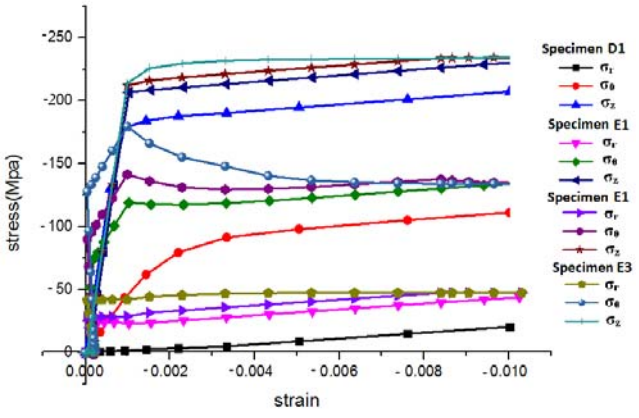


Fig. 19 Evolution of $\sigma_r$, $\sigma_\theta$, and $\sigma_z$ with increase of compression strain under different tension $\sigma_{\theta,pre}$

Table 11 Yield strength of core tube under compression with different tension $\sigma_{\theta,pre}$

| Model No. | $\sigma_{\theta,pre}$ (MPa) | Stresses at tension yielding | | | |
|---|---|---|---|---|---|
| | | $\sigma_\theta$ (MPa) | $\sigma_\theta/f_y$ | $\sigma_z$ (MPa) | $\sigma_z/f_y$ |
| F1 | 50 | -120 | 0.75 | -218 | 1.363 |
| F2 | 75 | -125 | 0.781 | -225 | 1.406 |
| F3 | 125 | -135 | 0.844 | -235 | 1.469 |

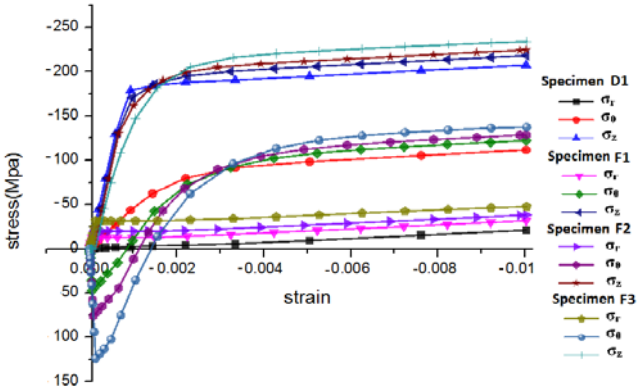


Fig. 20 Evolution of $\sigma_r$, $\sigma_\theta$, and $\sigma_z$ with increase of compression strain under different compression $\sigma_{\theta,pre}$

Three levels of tension $\sigma_{\theta,pre}$ in the core tube are studied, which are 50 MPa, 75 MPa and 125 MPa. When the core tube yields in compression, the tension $\sigma_{\theta,pre}$ reduces to about -120 MPa, which is 0.75 times of $f_y$, as listed in Table 11 and shown in Fig. 20. The compression strength of the core tube in $z$ direction increases to about 218 MPa, which is about 1.363 times of $f_y$. That is, effects of tension $\sigma_{\theta,pre}$ on compression strength of the core tube is nearly the same with that of compression $\sigma_{\theta,pre}$.

## 6. Hysteretic behavior of TTBRBs

### *6.1 Hysteretic behavior of TTBRBs with different gap width*

The gap between tubes exists inevitably, for the manufacture error. On one hand, the gap reduces the stiffness provided by the restraining tubes and the core tube might be encountered local buckling. On the other hand, the gap hinders the developing of circumference in core tube, which affects the tension/compression strength in $z$ direction of the core tube.

TTBRBs with and without gaps are studied as listed in Table 12. The gap width of 5 mm is selected through trial and error, which could provide flexural restraint to the core tube to prevent it from global buckling, and would not restrain its deformation in radius direction. The length of TTBRB is 9000 mm.

For the existence of a gap with width of 5mm in Model

Table 12 Parameters of TTBRBs for studying effects of gap width on hysteretic behavior

| Model No. | $r$ (mm) | $t$ (mm) | $t_1$ & $t_2$ (mm) | $a_1$ (mm) | $a_2$ (mm) |
|---|---|---|---|---|---|
| A-1 | 100 | 10 | 13 | 0 | 0 |
| D-1 | 100 | 10 | 13 | 5 | 0 |
| D-2 | 100 | 10 | 13 | 0 | 5 |
| D-3 | 100 | 10 | 13 | 5 | 5 |

Table 13 Parameters of TTBRBs for studying effects of $\sigma_{\theta,pre}$ on hysteretic behavior

| Model No. | $r$ (mm) | $t$ (mm) | $t_1$ & $t_2$ (mm) | $\sigma_{\theta,pre}$ in core tube (MPa) |
|---|---|---|---|---|
| M-1 | 200 | 10 | 26 | 0 |
| M-2 | 200 | 10 | 26 | -125 |
| M-3 | 200 | 10 | 26 | 135 |

D-3, the radius deformation of the core tube in tension/compression is not restrained by the outer and inner restraining tubes. Compared with model A-1 whose strength is increased due to the restrained radius shrinkage or expansion, hysteretic loops of D-3 is squeezed obviously, as shown in Fig. 21(a). The tension/compression resistance reduces about 200 kN, which is reduced from 1200 kN to 1000 kN. At the same time, the core tube might encounter local buckling for a TTBRB with a great gap width, as shown in Fig. 22, which greatly degrades the behavior of a TTBRB as a seismic energy dissipation element.

If there is a gap only between the core tube and the outer tube, like D-1, or between the core tube and the inner tube, like D-2, the restraining tubes could provide restraints to the core tube when it is in tension or in compression. Hence the tension or the compression strength of the core tube is improved, as shown in Fig. 21(b).

### 6.2 Hysteretic behavior of TTBRBs with different circumference pre-stress

TTBRBs for studying effects of $\sigma_{\theta,pre}$ on the hysteretic behavior are listed in Table 13. The length is 9000 mm. Three levels $\sigma_{\theta,pre}$ are studied, which are 0 MPa, -125 MPa and 135 MPa.

There is tension $\sigma_{\theta,pre}$ in the core tube of M-3. Compared with M-1, hysteretic curves are more fully developed, especially when the TTBRB is in compression, as shown in Fig. 23(a). Whether the $\sigma_{\theta,pre}$ is tension or compression has nearly no influences on the hysteretic behavior of a TTBRB, as shown in Fig. 23(b).

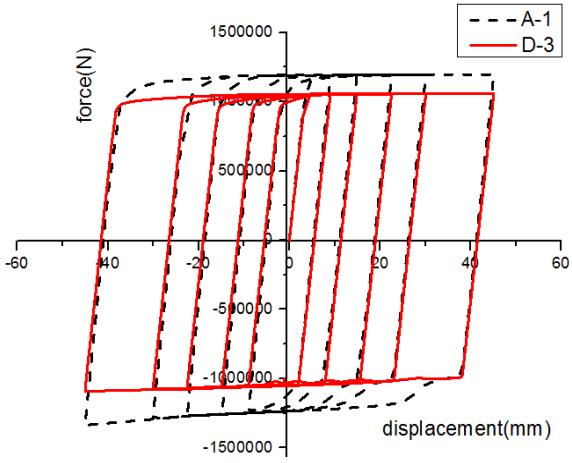


(a) Comparison of hysteretic behavior between model A-1 and D-3

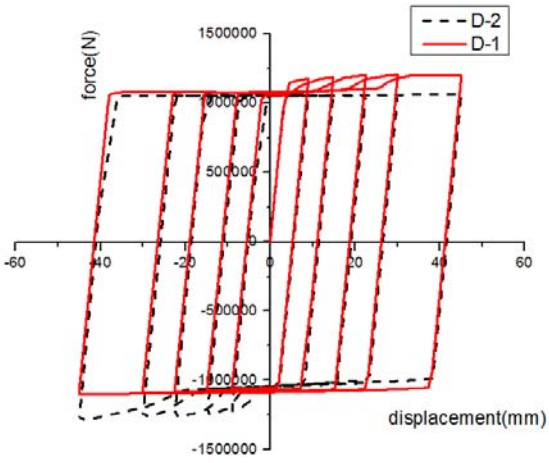


(b) Comparison of hysteretic behavior between model D-1 and D-2

Fig. 21 Hysteretic behavior of TTBRBs with different gap width

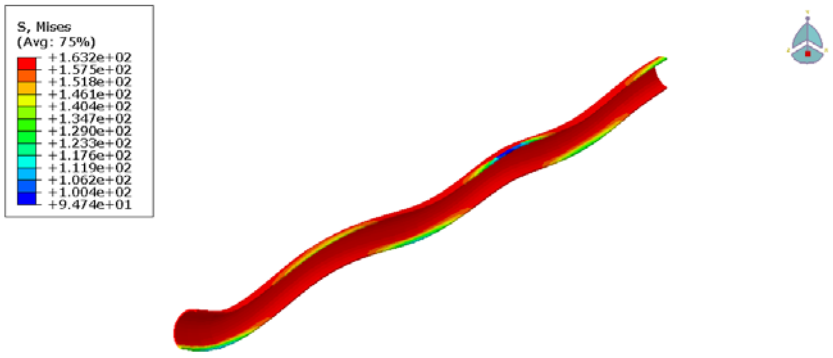


Fig. 22 Local buckling of core tube of model D-3

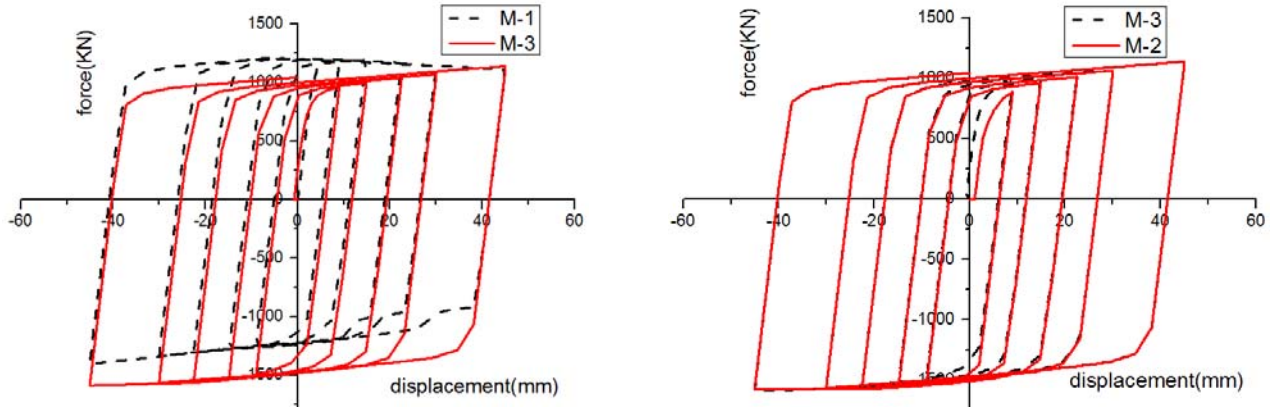


(a) Comparison of hysteretic behavior between model M-1 and M-3 (b) Comparison of hysteretic behavior between model M-2 and M-3

Fig. 23 Hysteretic behavior of TTBRBs with different circumference pre-stress

## 7. Conclusions

The behavior of the Three-Tube Buckling-Restrained Brace (TTBRB) with circumference pre-stress in core tube are investigated through a verified FEM. The TTBRB is composed of one core tube in the middle and two restraining tubes that are outside and inside the core tube, respectively, to restrain the global and local buckling of the core tube. Compare with a BRB with a solid section core, the tube has much higher gyration radius and the self-weight could be greatly reduced. The core tube consists of two non-yielding parts at the two ends and one yielding part in the middle. UHMWPE tubes are installed between the tubes to reduce the friction when the core tube is axially elongated or shortened. One-sided bolts at the end of the TTBRB works as stoppers to maintain the relative positions of the three tubes.

Based on yield criteria of fringe fiber, a design method for restraining tubes is proposed. The proposed design method is applicable for TTBRBs with different radius-thickness ratios, with different gap widths between core tube and restraining tubs and $\sigma_{\theta,pre}$.

The outer and inner tubes would restrain the deformation of the core tube in radius direction, which causes circumference stress ($\sigma_\theta$) in the core tube. Together with the $\sigma_{\theta,pre}$ in the core tube that is applied through interference fit of the three tubes, the yield strength of the core tube in axial direction could be improved from 160 MPa to 235 MPa.

Effects of gap width between core tube and restraining tubes and $\sigma_{\theta,pre}$ on the hysteretic behavior of TTBRBs are presented. Analysis results show that the gap width and the $\sigma_{\theta,pre}$ could significantly affect the hysteretic behavior of a TTBRB. The hysteretic behavior of a TTBRB with gap are much squeezed, compared with those without gap. It has nearly no influences on the hysteretic behavior of a TTBRB whether the circumference pre-stress is tension or compression.

## Acknowledgments

The authors wish to acknowledge the support from the National Natural Science Foundation of China (51578322, 51608305) for the work reported in this paper.

## References

Atlayan, Q. and Charney, A.F. (2014), "Hybrid buckling-restrained braced frames", *J. Constr. Steel Res.*, **96**(1), 95-105.

Chen, Q., Wang, C.L., Meng, S. and Zeng, B. (2016), "Effect of the un-bonding materials on the mechanic behavior of all-steel buckling-restrained braces", *Eng. Struct.*, **111**(4), 478-493.

Chou, C.C., Chung, P.T. and Cheng, Y.T. (2016), "Experimental evaluation of large-scale dual-core self-centering braces and sandwiched buckling-restrained braces", *Eng. Struct.*, **116**(1), 12-25.

Dongbin, Z., Xin, N., Peng, P., Mengzi, W., Kailai, D. and Yabin, C. (2016), "Experimental study and finite element analysis of a buckling-restrained brace consisting of three steel tubes with slotted holes in the middle tube", *J. Constr. Steel Res.*, **124**(1), 1-11.

Ghowsi, A.F. and Sahoo, D.R. (2015), "Fragility assessment of buckling-restrained braced frames under near-field earthquakes", *Steel Compos. Struct., Int. J.*, **19**(1), 173-190.

Guerrero, H., Ji, T., Escobar, J.A. and Teran-Gilmore, A. (2018), "Effects of Buckling-Restrained Braces on reinforced concrete precast models subjected to shaking table excitation", *Eng. Struct.*, **163**(1), 294-310.

Heidary-Torkamani, H. and Maalek, S. (2017), "Conceptual numerical investigation of all-steel Tube-in-Tube buckling restrained braces", *J. Constr. Steel Res.*, **139**(1), 220-235.

Hosseinzadeh, S.H. and Mohebi, B. (2016), "Seismic evaluation of all-steel buckling restrained braces using finite element analysis", *J. Constr. Steel Res.*, **119**(1), 76-84.

Hoveidae, N., Tremblay, R., Rafezy, B. and Davaran, A. (2015), "Numerical investigation of seismic behavior of short-core all-steel buckling restrained braces", *J. Constr. Steel Res.*, **114**(1), 88-99.

Judd, J.P., Marinovic, I., Eatherton, M.R., Hyder, C., Phillips, A.R., Tola, A.T. and Charney, F.A. (2016), "Cyclic tests of all-steel web-restrained buckling-restrained brace subassemblages", *J. Constr. Steel Res.*, **125**(1), 164-172.

Kim, S.H. and Choi, S.M. (2015), "Structural behavior of inverted V-braced frames reinforced with non-welded buckling restrained braces", *Steel Compos. Struct., Int. J.*, **19**(6), 1581-1598.

Mirtaheri, S.M., Nazeryan, M., Bahrani, M.K., Nooralizadeh, A., Montazerian, L. and Naserifard, M. (2017), "Local and global

buckling condition of all-steel buckling restrained braces", *Steel Compos. Struct., Int. J.*, **23**(2), 217-228.
Momenzadeh, S., Seker, O., Faytarouni, M. and Shen, J. (2017), "Seismic performance of all-steel buckling-controlled braces with various cross-sections", *J. Constr. Steel Res.*, **139**(1), 44-61.
Ozcelik, R., Dikiciasik, Y. and Erdil, E.F. (2017), "The development of the buckling restrained braces with new end restrains", *J. Constr. Steel Res.*, **138**(1), 208-220.
Piedrafita, D., Cahis, X., Simon, E. and Comas, J. (2015), "A new perforated core buckling restrained brace", *Eng. Struct.*, **85**(1), 118-126.
Speicher, M.S. and Harris, J.L. (2018), "Collapse Prevention seismic performance assessment of new buckling-restrained braced frames using ASCE 41", *Eng. Struct.*, **164**(1), 274-289.
Sutcu, F., Takeuchi, T. and Matsui, R. (2014), "Seismic retrofit design method for RC buildings using buckling-restrained braces and steel frames", *J. Constr. Steel Res.*, **101**(10), 304-313.
Takahashi, S. and Mochizuki, N. (1979), "Experimental study on buckling of un-bonded braces under axial compressive force: part 1. Summaries of technical papers of annual meeting", *Japan: Arch. Inst. Japan*, pp. 1623-1626.
Tremblay, R., Bolduc, P., Neville, R. and DeVall, R (2006), "Seismic testing and performance of buckling restrained bracing systems", *Can. J. Civil Eng.*, **33**(1), 183-198.
Zhang, D., Nie, X., Pan, P., Wang, M., Deng, K. and Chen, Y. (2016), "Experimental study and finite element analysis of a buckling-restrained brace consisting of three steel tubes with slotted holes in the middle tube", *J. Constr. Steel Res.*, **124**(1), 1-11.

*CC*